# A Novel Three-Phase Three-Port UPS Employing a Single High-Frequency Isolation Transformer


Chuanhong Zhao and Johann W. Kolar

ETH Zurich, Power Electronic Systems Laboratory
ETH Zentrum / ETL H22, Physikstr. 3, CH-8092 Zurich / SWITZERLAND
Tel.: +41-1-632 2834 Fax.: +41-1-632 1212
Email: kolar@lem.ee.ethz.ch



*Abstract* — **A three-phase PWM rectifier and a three-phase PWM inverter are coupled via two four-quadrant full-bridge converter cells and a high-frequency isolation transformer. By employing a third transformer winding and further full-bridge cell battery energy storage is incorporated into the power transfer between rectifier and inverter resulting in a *Three-Port UPS* concept. The phase shift control of the power flow between the ports is analyzed for square-wave operation of the full-bridge cells. Furthermore, the utilization of the degrees of freedom of the system control, i.e. the extension to duty cycle control for optimizing the system behavior is discussed and control laws ensuring minimum overall system losses are derived. Finally, a control-oriented converter model is proposed and the decoupled control of the power flow of the ports is treated briefly. All theoretical considerations are verified by simulations using PSIM.**


## I. INTRODUCTION

Highly reliable three-phase on-line uninterrupted power supply systems (UPS) are formed by back-to-back connection, i.e. DC side coupling of a mains-side voltage source rectifier and a load-side voltage source inverter [1]. There, the battery energy storage is directly connected to the DC link or coupled via a DC/DC converter in order to allow a control of the charging or discharging current and a compensation of battery voltage changes. Furthermore, for safety reasons and voltage level adaption in general a 50/60Hz isolation transformer is employed on the input or output side which, however, constitutes a significant drawback concerning volume/weight, costs and efficiency.

In this paper a novel UPS concept with high frequency isolation of a three-phase PWM rectifier stage (system/port 1), a three-phase PWM inverter stage (system/port 2) and a battery energy storage (system/port 3) is proposed, [2] (cf. **Fig.1**). There, port 1, port 2 and port 3 are coupled via three four-quadrant full-bridge converter cells operating in phase-shift mode and a single three-winding transformer. Accordingly, the system will be denoted as *Three-Port UPS* in the following.

For realizing the three-phase rectifier and inverter function of the system *20* (*6+4+4+6*) power transistors with anti-parallel diodes have to be employed. Therefore, the realization effort is lower than, e.g. for a three-phase high-frequency link AC/AC matrix converter comprising *24* transistors and diodes [4]. As further advantage one has to point out the continuous shape of the input *and* output currents and the decoupling of the mains and the load concerning power and voltage fluctuations in case sufficient DC link capacitance $C_1$ and $C_2$ is provided for the rectifier and/or the inverter. Alternatively, $C_1$ and $C_2$ could be realized as foil capacitors ensuring only a constant DC link voltage level for switching transients.

The system shown in Fig.1 in general allows a bidirectional energy conversion between two three-phase voltage systems and a DC voltage source and therefore is of potential interest also in connection with future distributed generator of electric energy. There, the mains could, e.g. be formed by a wind turbine or a variable frequency generator powered by a micro turbine where the battery storage could compensate power fluctuations of the regenerative energy sources. Also, further other storage elements like flywheels or SMES or a fuel cell or photovoltaic generator could be incorporated in parallel by individual full-bridge converter cells and related transformer windings. An interesting application area of such X-port UPS-type converter system would e.g. be future intelligent nodes of the energy distribution system which also could be extended to a power quality control centre [5] featuring symmetrization of unbalanced loads and active filtering of mains voltage or load current harmonics.

The control of the power flow in the three-port system is in the simplest case by proper phase shift of the individual full-bridge cells operating in square-wave mode. In **Section II** the system control characteristics are determined based on the equivalent circuit of a three-winding transformer [6] and the dependency of the power transfer between two full-bridge cells on the phase displacement of the control signals. There, in a first step a turns ratio of $N_1$:$N_2$:$N_3$=1:1:1 is assumed and the PWM rectifier, the PWM inverter and the voltage-type energy storage are replaced by equal

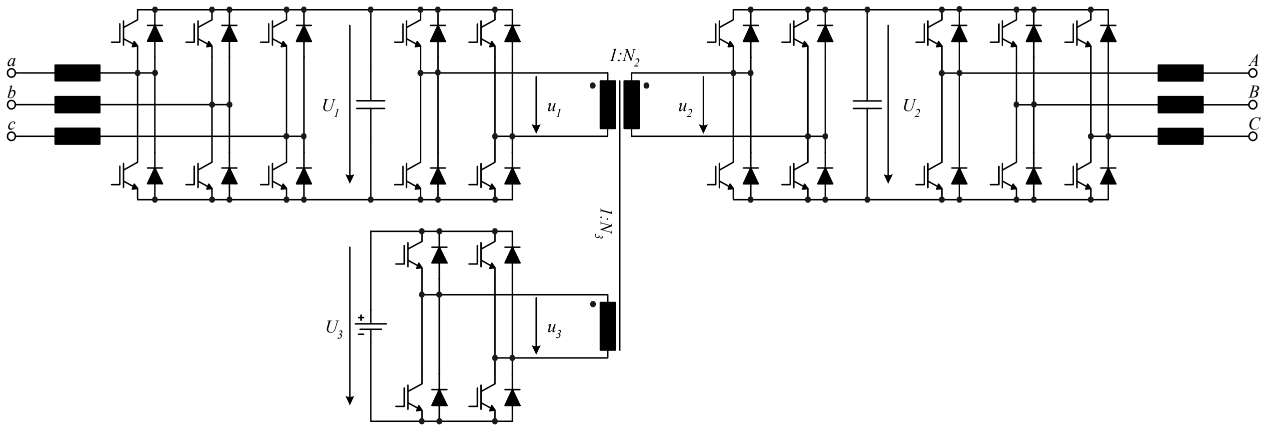


**Fig.1:** Proposed three-phase three-port high-frequency link converter (*Three-Port UPS, [2]*). The high frequency coupling of multiple four-quadrant full-bridge converter cells via a single transformer has been shown in principle in [3] (cf. Fig.8 in [3]), however, no procedure for controlling the system has been given there.

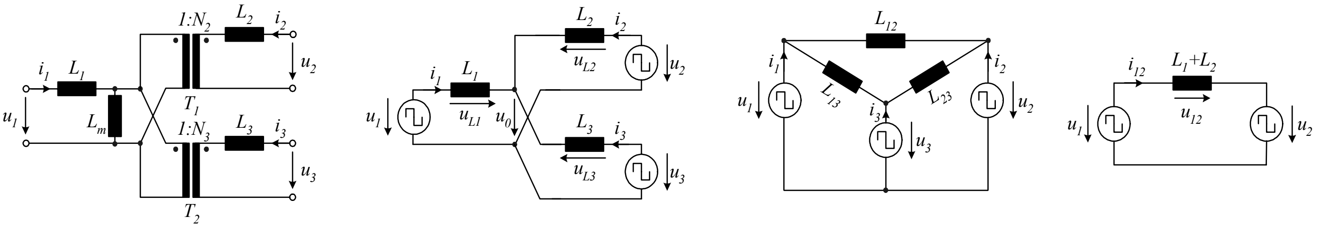

**Fig.2: (a)** Equivalent circuit of a three-winding transformer; **(b)** Y-equivalent circuit of the proposed converter used for analyzing the dependency of the power transfer between the ports on the control signal phase displacements; **(c)** Δ-equivalent circuit of the three-port system; **(d)** equivalent circuit for studying the power flow between two ports when the third port is opened.

voltage sources $U_1$=$U_2$=$U_3$; subsequently the considerations are generalized to different DC voltages. It is shown that a zero net power flow can be achieved for one port while power is transferred between the two other ports. The introduction of duty cycle control for minimizing the overall system conduction and switching losses is discussed in **Section III**. The converter control using a decoupling network is treated briefly in **Section IV**. Finally, in **Section V** the theoretical considerations are verified by simulations using PSIM.

## II. Controllability of the Power Flow in the Three-Port Converter

### *A. Equivalent Circuit of a Three-Winding Transformer*

The equivalent circuit of a three-winding transformer given in [6], is shown in **Fig.2**(a) where $L_m$ is the effective magnetizing inductance and $T_1$ and $T_2$ are two ideal transformers with turn ratios $1{:}N_2$ and $1{:}N_3$. The transformer leakage inductances which are determining the power transfer in connection with the phase displacement of the individual full-bridge converter cell control signals are represented by $L_1$, $L_2$, and $L_3$.

The parameters of the equivalent circuit can be derived from the measured values of the self inductances $Z_1$, $Z_2$, $Z_3$ and the mutual inductances $M_{12}$, $M_{13}$, and $M_{23}$ of the transformer windings

$$\begin{aligned} &N_2 = \frac{M_{23}}{M_{13}} \quad N_3 = \frac{M_{23}}{M_{12}} \quad L_m = \frac{M_{12}M_{13}}{M_{23}} \\ &L_1 = Z_1 - L_m \quad L_2 = Z_2 - N_2^2 L_m \quad L_3 = Z_3 - N_2^3 L_m \end{aligned} \tag{1}$$

### *B. Direction of the Converter Power Flow*

For limiting to the essentials we represent the output voltages of the full-bridge cells by square wave voltage sources with a duty cycle of 0.5. Furthermore, we assume $N_2$ and $N_3$ to be equal to 1 and neglect the transformer magnetizing current and/or magnetizing inductance.

The resulting equivalent circuit of the proposed system is shown in Fig.2(b). The phase shift of control signals of two full-bridge cells and/or of the square wave voltage sources $u_1$ and $u_2$ is denoted as $\phi_2$ in the following; accordingly, $\phi_3$ denotes the phase displacement of $u_1$ and $u_3$. There, $\phi_2$ and/or $\phi_3$ are defined as positive when $u_1$ is leading $u_2$ and/or $u_1$ is leading $u_3$. The control range of $\phi_2$ and $\phi_3$ is from $-\pi/2$ to $\pi/2$.

The three-port converter can be simplified to a two-port converter if the third port is open. Based on [3] we then have for the power flow between two full-bridge phase-shift controlled converter cells (cf. Fig.2(d))

$$P_{12} = \frac{\phi_2(\pi - \phi_2)V_1V_2T_s}{2\pi^2(L_1 + L_2)} \tag{2}$$

where $V_1$ *and* $V_2$ are the DC voltages of the converters generating $u_1$ *and* $u_2$ and $T_s$ denotes the switching cycle. According to (2) the amount and direction of the power flow is determined by the phase shift $\phi_2$.

This is also immediately clear from a phasor diagram of the fundamentals of the voltages and currents which is depicted in **Fig.3**. The fundamental power transferred from port 1 and/or $u_1$ to port 2 and/or $u_2$ is

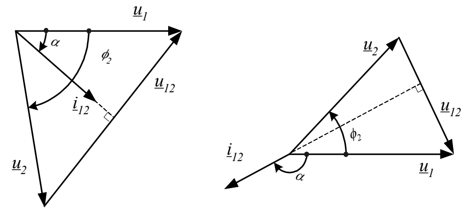

**(a)** $\phi_2 > 0$ **(b)** $\phi_2 < 0$

**Fig.3:** The phasor diagram of the fundamentals of the voltages and currents when the third port is open

$$P_{12} = \frac{1}{2}\hat{U}_1\hat{I}_{12}\cos(\alpha) = \frac{1}{2}\hat{U}_1\frac{\hat{U}_{12}}{\omega(L_1 + L_2)}\cos(\alpha) \tag{3}$$

where $\hat{U}_1$=4/π$V_1$, $\hat{U}_2$=4/π$V_2$, $\hat{U}_{12}$ is the absolute value of $\underline{u}_{12}=\underline{u}_1-\underline{u}_2$, $\omega=2\pi/T_S$ and $\alpha$ denotes the phase displacement of $\underline{u}_1$ and the current $\underline{i}_{12}$ which is oriented perpendicular to $\underline{u}_{12}$. For $\phi_2 > 0$ (cf. Fig.3(a)), and/or in case $u_1$ is leading $u_2$, $\alpha$ is smaller than π/2. Therefore, we have $P_{12}>0$, the power flow is physically oriented from port 1 and/or $u_1$ to port 2 and/or $u_2$ and reverses for $\phi_2 < 0$ since $\alpha$ then is larger than π/2 (cf. Fig.3(b)).

The Y-equivalent circuit depicted in Fig.2(b) can be transformed into a Δ-equivalent circuit [7] shown in Fig.2(c) which allows to determine the resulting power flow of the three-port system by superposition of the power transfer of three two-port systems $u_1$,$u_2$, $u_1$,$u_3$, *and* $u_2$,$u_3$. E.g., for $\phi_2 > 0$, $\phi_3 > 0$ and $\phi_2 > \phi_3$ (cf. **Fig.4** (a)) the power flow is from $u_1$ to $u_2$, $u_1$ to $u_3$ and $u_3$ to $u_2$ as $\phi_2 > \phi_3$. Therefore, $u_1$ is acting as a source and $u_2$ is consuming power. Dependent on the relation of $\phi_2$ *and* $\phi_3$ and of $V_1$, $V_2$ *and* $V_3$, Port 3 and/or $u_3$ can be sinking or sourcing power or remain at zero power.

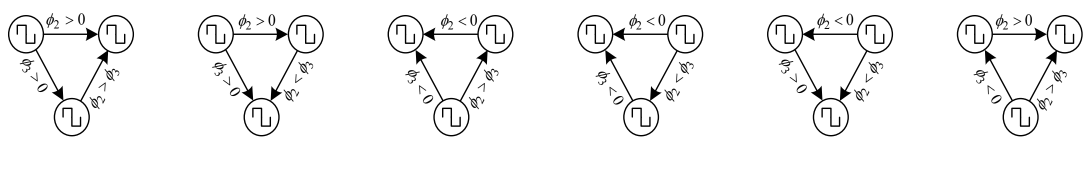

**Fig.4:** Equivalent circuit for studying the power flow between three ports. The direction of power flow is only determined by $\phi_2$, $\phi_3$, not by $V_1$, $V_2$ and $V_3$.

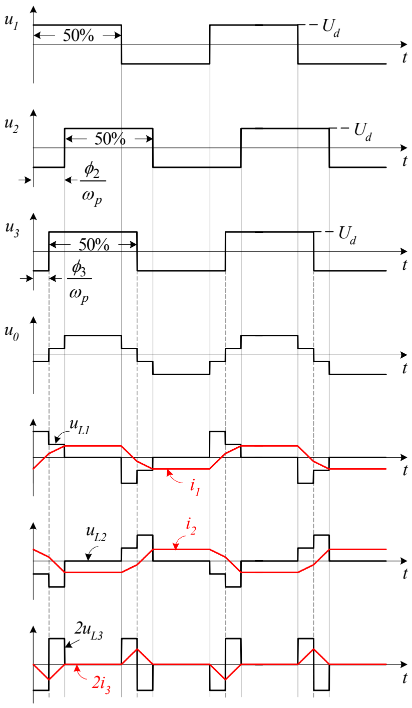


**Fig.5:** Key waveforms for achieving zero net power flow to port 3 assuming equal levels of the full-bridge converter cell DC voltages, i.e. $V_1$=$V_2$=$V_3$=$U_d$.

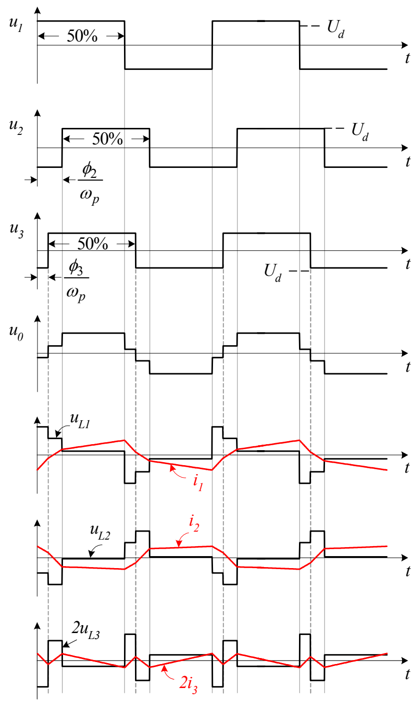


**Fig.6:** Key waveforms for $P_3$ = 0 and/or $P_1$ =−$P_2$ =$P$ for differing levels of the full-bridge converter cell DC voltages $V_1$, $V_2$, $V_3$.

In summary, a power transfer is possible in any direction between any ports simultaneously and the direction is only determined by $\phi_2$, and $\phi_3$ (cf. Fig.4).

### C. Control Leaving One Port at Zero Average Power

An important function of an UPS system is to directly supply power from the mains to the load without charging or discharging the battery energy storage. For the three-port UPS this cannot be realized at low battery voltage even if all power transistors of the battery port full-bridge cell are remaining in the off-state as the anti-parallel free-wheeling diodes would be forced into conduction by high output voltages of the mains or load port full-bridge cells. Therefore, $\phi_2$ and $\phi_3$ have to be selected properly in order to achieve $P_3 = 0$ and a given value of $P_1 = -P_2 = P$ (since the sum of the power of three voltage sources has to be zero, $P_1$+$P_2$+$P_3$=0, if losses are neglected).

As the currents in the leakage inductances are directly the currents of the voltage sources of the Y-equivalent circuit, the following considerations are referring to Fig.2(b). Here, again $\phi_2 > 0$, $\phi_3 > 0$ and $\phi_2 > \phi_3$ is assumed. The key waveforms resulting in $P_3 = 0$ are shown in **Fig.5** for $V_1$=$V_2$=$V_3$ and for the general case of different DC voltage levels $V_1$, $V_2$, $V_3$ in **Fig.6**. According to the law of superposition, $u_0$ contained $u_1$, $u_2$, $u_3$ is

$$u_0 = \frac{u_1 L_1 L_2 + u_2 L_1 L_3 + u_3 L_1 L_2}{L_1 L_2 + L_1 L_3 + L_2 L_3} \tag{4}$$

For the power flow of the ports we then have

$$\begin{aligned}
P_1 &= \frac{\phi_2(\pi-\phi_2)V_1V_2L_3 + \phi_3(\pi-\phi_3)V_1V_3L_2}{2\pi^2(L_1L_2+L_1L_3+L_2L_3)}T_s \\
P_2 &= \frac{\phi_2(\phi_2-\pi)V_1V_2L_3 + (\phi_2-\phi_3)(\phi_2-\phi_3-\pi)V_2V_3L_1}{2\pi^2(L_1L_2+L_1L_3+L_2L_3)}T_s \\
P_3 &= \frac{\phi_3(\phi_3-\pi)V_1V_3L_2 + (\phi_2-\phi_3)(\pi-\phi_2+\phi_3)V_2V_3L_1}{2\pi^2(L_1L_2+L_1L_3+L_2L_3)}T_s
\end{aligned} \tag{5}$$

From (5) now the relation of $P$ *and* $\phi_2$ and of $\phi_2$ *and* $\phi_3$ can be derived under the side condition of $P_3$=0 and $P_1$=−$P_2$=$P$. As shown in **Fig.7** and **Fig.8** for $V_1$=500V, $V_2$=400V, $V_3$=360V, $P_1$=−$P_2$=5kW, $P_3$=0, $L_1$=$L_2$=$L_3$=100µH, and $f_s$=20kHz, there are two solutions for $\phi_2$ and $\phi_3$. As a higher phase shift $\phi_2$ and $\phi_3$ result in a higher peak value of the current in the corresponding leakage inductance and/or in higher conduction and switching losses the lower phase shift values $\phi_{21}$ and $\phi_{31}$ which have to be selected for the system control.

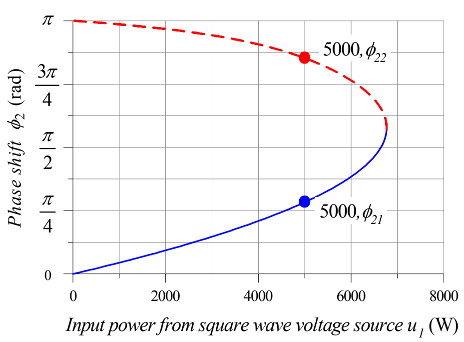


**Fig.7**: Phase shift $\phi_2$ for achieving $P_1$=−$P_2$=5kW and $P_3$=0. Operating parameters: $V_1$=500V, $V_2$=400V, $V_3$=360V, $L_1$=$L_2$=$L_3$=100µH, and $f_s$=20kHz.

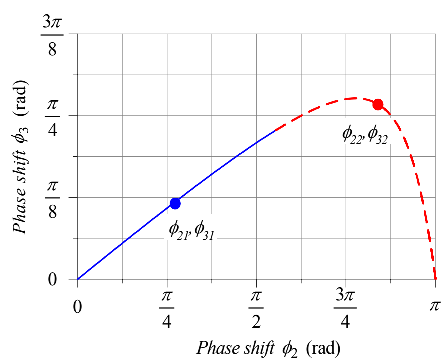


**Fig.8:** Dependency of phase shift $\phi_3$ on $\phi_2$ for achieving zero net power flow to port 3, i.e. $P_3$=0 (cf. Fig.7). Operating parameters: as for Fig.7.

## III. MINIMIZATION OF THE OVERALL SYSTEM LOSSES

### A. *Introduction of Duty Cycle Control*

In order to gain degrees of freedom for minimizing the overall system losses, duty cycle variation of the full-bridge converter cell output voltages $u_1$, $u_2$ and $u_3$ could be introduced in addition to phase shift control as shown in **Fig.9**. There, the control range of $\delta_1$, $\delta_2$ and $\delta_3$ is from 0 to $\pi/2$.

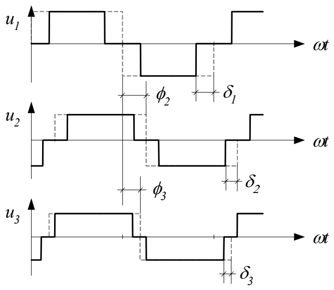


**Fig.9:** Definition of phase displacement and duty cycle of the converter cell output voltages $u_1$, $u_2$ and $u_3$.

### B. *Zero Circulating Power*

The power transferred from $u_1$ to $u_2$, from $u_2$ to $u_3$ and from $u_3$ to $u_1$ will be denoted as $P_{12}$, $P_{23}$ and $P_{31}$ in the following. Aiming for minimizing losses a circulation of power inside the system which would not contribute to the power flow of the ports has to be prevented, i.e.

$$P_{12}+P_{23}+P_{31} = 0 \tag{6}$$

has to be ensured. Considering $P_2 = P_{21}+P_{23}$ and $P_3 = P_{31}+P_{32}$, we have for $P_{12}$, $P_{23}$, and $P_{31}$ in dependency on $P_2$, $P_3$ with (6)

$$\begin{aligned} P_{12} &= -\tfrac{2}{3}P_2 - \tfrac{1}{3}P_3 \\ P_{23} &= \tfrac{1}{3}P_2 - \tfrac{1}{3}P_3 \\ P_{31} &= \tfrac{1}{3}P_2 + \tfrac{2}{3}P_3 \end{aligned} \tag{7}$$

For the sake of simplicity the further considerations are restricted to fundamentals of the voltages and currents. Furthermore, $L_{12}=L_{13}=L_{23}$, $\phi_2>0$, $\phi_3>0$ and $\phi_2>\phi_3$ is assumed. The corresponding phasor diagram is shown in **Fig.10** where $\underline{u}_1$ defines the orientation of the real axis

$$\underline{u}_1 = \hat{U}_1 + 0j \tag{8}$$

We then have for $P_{12}$

$$P_{12} = \frac{1}{2}\hat{U}_1\hat{I}_{12}\cos(\alpha) = \frac{\hat{U}_1}{2\omega L_{12}}\hat{U}_{12}\cos(\alpha) \tag{9}$$

Considering the phase displacement $\phi_2$ of $u_1$ and $u_2$ (cf. Fig.9) and/or of $\underline{u}_1$ and $\underline{u}_2$, $\underline{u}_2$ can be expressed as (cf. Fig.10)

$$\underline{u}_2 = \hat{U}_2\cos(\phi_2) - \hat{U}_2\sin(\phi_2)j \tag{10}$$

Accordingly, $\underline{u}_{12}$ formed by $\underline{u}_1$ and $\underline{u}_2$ is

$$\begin{aligned} \underline{u}_{12} &= \underline{u}_1 - \underline{u}_2 \\ &= \hat{U}_1 - \hat{U}_2\cos(\phi_2) + \hat{U}_2\sin(\phi_2)j \end{aligned} \tag{11}$$

Introducing the phase displacement $\alpha$ of $\underline{u}_1$ and $\underline{i}_{12}$, $\underline{u}_{12}$ which is leading $\underline{i}_{12}$ by $\pi/2$ can be alternatively formulated as

$$\begin{aligned} \underline{u}_{12} &= \hat{U}_{12}\cos(\tfrac{\pi}{2}-\alpha) + \hat{U}_{12}\sin(\tfrac{\pi}{2}-\alpha)j \\ &= \hat{U}_{12}\sin(\alpha) + \hat{U}_{12}\cos(\alpha)j \end{aligned} \tag{12}$$

Combining (11) and (12) results in

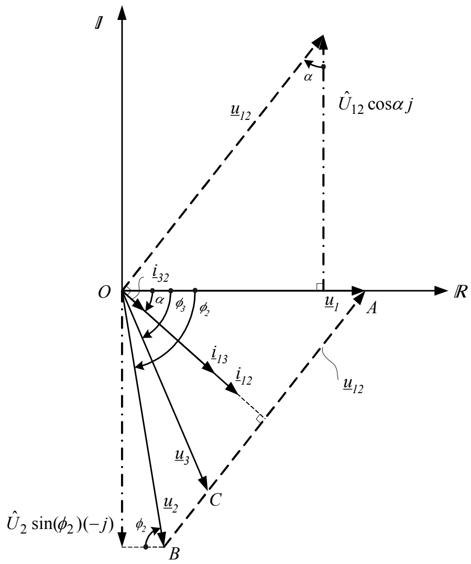


**Fig.10:** Phasor diagram of the fundamentals of the system voltages and currents.

$$\hat{U}_{12}\cos(\alpha) = \hat{U}_2\sin(\phi_2) \tag{13}$$

Considering (13), the power flow $P_{12}$ (cf. (9)) now can be represented as

$$P_{12} = \frac{1}{2}\frac{\hat{U}_1}{\omega L_{12}}\hat{U}_{12}\cos\alpha = \frac{1}{2}\frac{\hat{U}_1}{\omega L_{12}}\hat{U}_2\sin(\phi_2) \tag{14}$$

Taking finally into account that the area $S_{\Delta OAB}$ of the triangle $\Delta_{OAB}$ in Fig.10 is

$$S_{\Delta OAB} = \tfrac{1}{2}\hat{U}_1\hat{U}_2\sin(\phi_2) \tag{15}$$

the power transferred between two ports in general is proportional to the area of the triangle defined by the phasors of the voltages of the ports and is inversely proportional to the equivalent impedance and/or inductance connecting the ports (cf. Fig.2c),

$$P_{12} = \frac{1}{2}\frac{\hat{U}_1}{\omega L_{12}}\hat{U}_2\sin(\phi_2) = \frac{1}{\omega L_{12}}S_{\Delta OAB} \tag{16}$$

Accordingly, $P_{13}$ and $P_{32}$ can expressed as

$$P_{13} = \frac{1}{\omega L_{13}}S_{\Delta OAC} \qquad P_{32} = \frac{1}{\omega L_{23}}S_{\Delta OBC} \tag{17}$$

where $S_{\Delta OAC}$ denotes the area of the triangle $\Delta_{OAC}$ and $S_{\Delta OBC}$ denotes the area of the triangle $\Delta_{OBC}$. Considering $P_{12}+P_{23}+P_{31}=0$, and $L_{12}=L_{13}=L_{23}$ as assumed above, (17) yields in combination with (16)

$$\begin{aligned} P_{12}+P_{23}+P_{31} &= P_{12}-P_{32}-P_{13} \\ &= \frac{1}{\omega L_{12}}S_{\Delta OAB} - \frac{1}{\omega L_{23}}S_{\Delta OBC} - \frac{1}{\omega L_{13}}S_{\Delta OAC} \\ &= \frac{1}{\omega L_{12}}(S_{\Delta OAB} - S_{\Delta OBC} - S_{\Delta OAC}) \\ &= 0 \end{aligned} \tag{18}$$

Simplifying (18), results in

$$S_{\Delta OAB} = S_{\Delta OBC} + S_{\Delta OAC} \tag{19}$$

Accordingly, for preventing circulating power flow, the head of $\underline{u}_3$ shown as point $C$ in Fig.10 has to be located on the line $AB$ and/or $\underline{u}_{12}$ and $\underline{u}_{13}$ have to be aligned what results in an alignment of $\underline{i}_{12}$, $\underline{i}_{13}$, and $\underline{i}_1=\underline{i}_{12}+\underline{i}_{13}$ what considerably simplifies the closed-form system description.

*C. Range of $\phi_2$ and $\phi_3$*

Substituting $\omega=2\pi/T_s$, $\hat{U}_1=4/\pi\cdot V_1\cos(\delta_1)$, and $\hat{U}_2=4/\pi\cdot V_2\cos(\delta_2)$ in (14), $P_{12}$ can be represented as

$$\begin{aligned} P_{12} &= \frac{1}{2}\frac{\hat{U}_1}{\omega L_{12}}\hat{U}_2\sin(\phi_2) \\ &= \frac{4T_s}{\pi^3 L_{12}}V_1\cos(\delta_1)V_2\cos(\delta_2)\sin(\phi_2) \end{aligned} \tag{20}$$

Analogously, we have for $P_{13}$ and $P_{23}$

$$\begin{aligned} P_{13} &= \frac{4T_s}{\pi^3 L_{13}}V_1\cos(\delta_1)V_3\cos(\delta_3)\sin(\phi_3) \\ P_{23} &= \frac{4T_s}{\pi^3 L_{23}}V_2\cos(\delta_2)V_3\cos(\delta_3)\sin(\phi_3-\phi_2) \end{aligned} \tag{21}$$

Referring to (20) and (21) the duty cycles $\delta_1$, $\delta_2$, and $\delta_3$ now can be expressed as

$$\begin{aligned} \delta_1 &= \begin{cases} a\cos\left(\dfrac{\pi\sqrt{\pi P_{12}P_{13}L_{12}(\tan(\phi_3)-\tan(\phi_2))}}{2V_1\sqrt{P_{23}T_s\tan(\phi_2)\tan(\phi_3)}}\right) & if\,(\phi_2>\frac{\pi}{2})\wedge(\phi_3\le\frac{\pi}{2}) \\ \pi - a\cos\left(\dfrac{\pi\sqrt{\pi P_{12}P_{13}L_{12}(\tan(\phi_3)-\tan(\phi_2))}}{2V_1\sqrt{P_{23}T_s\tan(\phi_2)\tan(\phi_3)}}\right) & otherwise \end{cases} \\ \delta_2 &= a\cos\left(\frac{\pi^3 P_{12}L_{12}}{4T_sV_1V_2\cos(\delta_1)\sin(\phi_2)}\right) \\ \delta_3 &= a\cos\left(\frac{\pi^3 P_{13}L_{12}}{4T_sV_1V_3\cos(\delta_1)\sin(\phi_3)}\right) \end{aligned} \tag{22}$$

For controlling the system 5 degrees of freedom, i.e. the phase displacements $\phi_2$, $\phi_3$, and the duty cycles $\delta_1$, $\delta_2$ and $\delta_3$ are available. Defining the power flow of two ports, e.g. $P_2$ and $P_3$ and ensuring zero circulating power two degrees of freedom are remaining, i.e. the converter characteristics can be expressed in dependency of $\phi_2$ and $\phi_3$.

Taking into account the restriction of the argument of an inverse cosine function to $[-1, 1]$, (22) results in a limitation of the operating range of the converter and/or in a limitation of the admissible range of $\phi_2$ and $\phi_3$. E.g., there follows considering $\delta_1(\phi_2, \phi_3)$,

$$-1 \le \frac{\pi\sqrt{\pi P_{12}P_{13}L_{12}(\tan(\phi_3)-\tan(\phi_2))}}{2V_1\sqrt{P_{23}T_s\tan(\phi_2)\tan(\phi_3)}} \le 1 \tag{23}$$

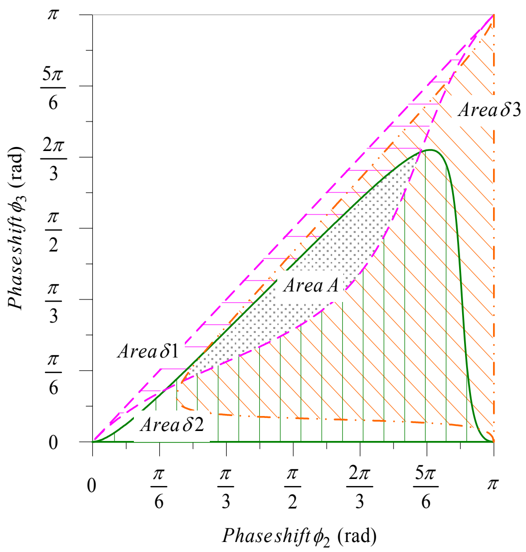


**Fig.11:** Operating *AreaA*, i.e. admissible range of phase shift $\phi_2$ and phase shift $\phi_3$ resulting form (22). Assumed operating parameters: $P_1$ = 4kW, $P_2$ = −3kW, $P_3$= −1kW, $V_1$=500V, $V_2$=400V, $V_3$=360V, $L_1$=$L_2$=$L_3$=100µH, and $f_s$=20kHz.

The corresponding range of $\phi_2$,$\phi_3$ is denoted as *Area*$\delta_1$ in the following (cf. **Fig.11**). In analogy, *Area*$\delta_2$ and *Area*$\delta_3$ are resulting from $\delta_2(\phi_2, \phi_3)$ and $\delta_3(\phi_2, \phi_3)$. Considering all restrictions, the system operation finally has to be restricted to the *AreaA* defined by the intersection of *Area*$\delta_1$, *Area*$\delta_2$ and *Area*$\delta_3$.

*D. Minimization of Overall System Losses*

For realizing the full-bridge converter cells in IGBT technology for a rated power in the range of 5…10kW, the system switching and conduction losses could be derived based on [10]. There, we have for the turn-on and turn-off energy loss of a power transistor and the turn-off energy loss of a power diode

$$\begin{aligned} w_{Soff}(u,i) &= K_{Soff1}\cdot u\cdot i + K_{Soff2}\cdot u\cdot i^2 + K_{Soff3}\cdot u^2 + K_{Soff4}\cdot u^2\cdot i + K_{Soff5}\cdot u^2\cdot i^2 \\ w_{Son}(u,i) &= K_{Son1}\cdot u\cdot i + K_{Son2}\cdot u\cdot i^2 + K_{Son3}\cdot u^2 + K_{Son4}\cdot u^2\cdot i + K_{Son5}\cdot u^2\cdot i^2 \\ w_{Doff}(u,i) &= K_{Doff1}\cdot u\cdot i + K_{Doff2}\cdot u\cdot i^2 + K_{Doff3}\cdot u^2 + K_{Doff4}\cdot u^2\cdot i + K_{Doff5}\cdot u^2\cdot i^2 \end{aligned} \tag{24}$$

where the indices $S$, $D$ denote whether the transistor or the diode is considered, and $u$ and $i$ are the voltage and the current being switched. The coefficients $K_i$ are determined by measurements and specified in [10].

For the conduction losses of the valves we have again according to [10]

$$\bar{p}_{S/D} = U_{F,S/D}\cdot\bar{i} + r_{S/D}\cdot i_{rms}^2 \tag{25}$$

where $\bar{\imath}$ denotes the average value and $i_{rms}$ is the rms value of the transistor or the diode current.

The overall system losses resulting for, e.g. $P_1$=4kW, $P_2$= −3kW, $P_3$= −1kW, $V_1$=500V, $V_2$=400V, $V_3$=360V, $L_1$= $L_2$=$L_3$= 100µH, and $f_s$ = 20kHz are shown in **Fig.12**. There, operating point $A$ results in minimum overall power semiconductor losses. This is clearly verified by operating point $B$ which is characterized by significantly higher current amplitudes and higher voltage *and* current phase displacements and/or significantly higher losses (cf. **Fig.13**).

Fig.13 also justifies the approximation of the actual current waveforms with the fundamentals (cf. (b) and (d)). Accordingly, the calculation of $\phi_2$ and $\phi_3$ based on (22) allows an accurate pre-control the system power flow (cf. **Fig.14**).

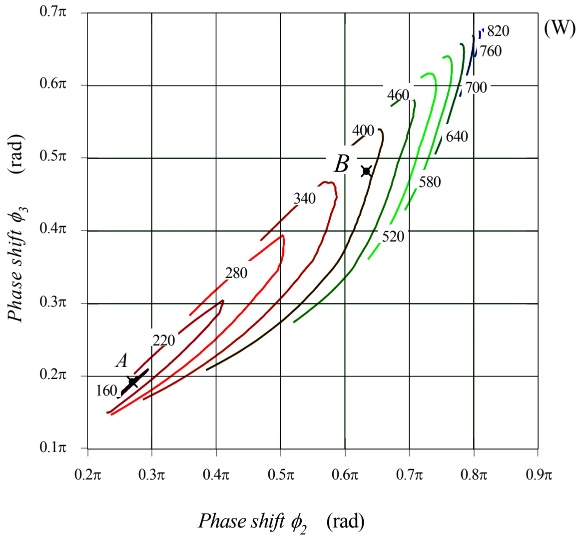


**Fig.12:** Overall system losses in dependency of $\phi_2$ and $\phi_3$. Assumed operating parameters: $P_1$ = 4kW, $P_2$ = −3kW, $P_3$= −1kW, $V_1$=500V, $V_2$=400V, $V_3$=360V, $L_1$=$L_2$=$L_3$=100µH, and $f_s$=20kHz.

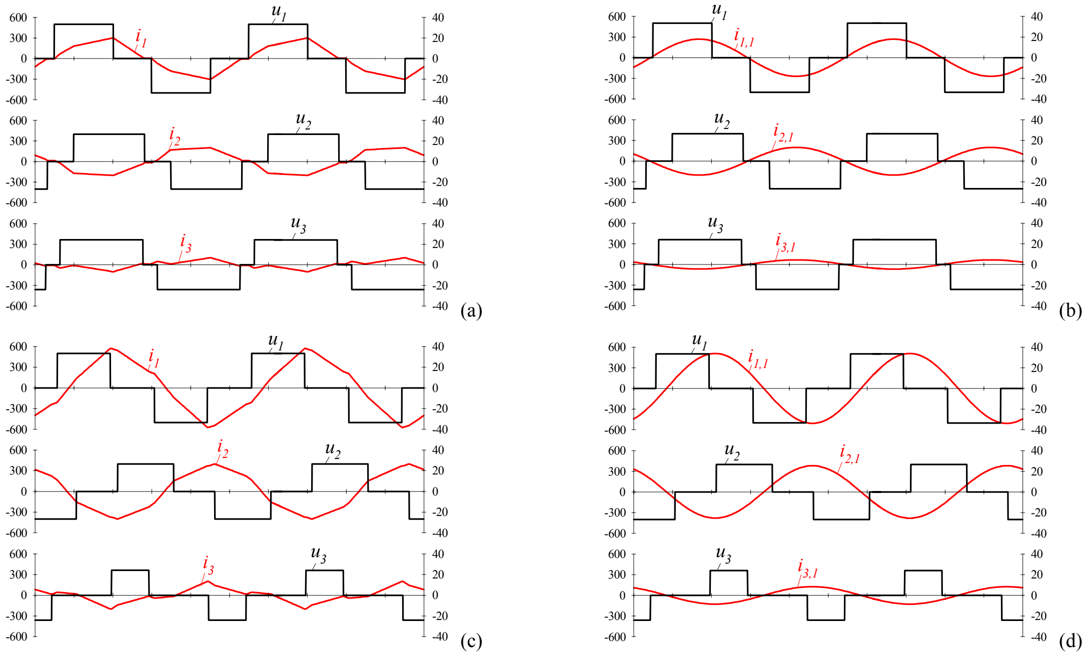


**Fig.13:** Actual time behavior of $u_1$, $u_2$, $u_3$ and $i_1$, $i_2$, $i_3$ (cf. (a) and (c)) and of the fundamental approximation of $i_{1,1}$, $i_{2,1}$, $i_{3,1}$ of $i_1$, $i_2$, $i_3$ (cf. (b) and (d)) for operation point $A$ (cf. **(a)** and **(b)**) and operation in point $B$ (cf. **(c)** and **(d)**) in Fig.12; Assumed operating parameters: $P_1$=4kW, $P_2$=−3kW, $P_3$=−1kW, $V_1$=500V, $V_2$=400V, $V_3$=360V, $L_1=L_2=L_3$=100µH, and $f_s$ = 20kHz. One has to note, that operating point $A$ in general is characterized by low switching losses.

## IV. CONTROL STRATEGIES

As mentioned in Section 3.C, two degrees of freedom, i.e. $\phi_2$ and $\phi_3$ are available for the system control. Accordingly, the system could be considered as a two input ($\phi_2$ and $\phi_3$) and two output ($P_2$ and $P_3$) control system.

The power $P_2$ of port 2 is the sum of $P_{21}$ (cf. (20)) and $P_{23}$ (cf. (21))

$$\begin{aligned} P_2 &= P_{21} + P_{23} = -P_{12} + P_{23} \\ &= K_1 \sin(\phi_2) + K_2 \sin(\phi_3 - \phi_2) \end{aligned} \tag{26}$$

where $K_1 = -\dfrac{4T_s}{\pi^3 L_{12}} V_1 \cos(\delta_1) V_2 \cos(\delta_2)$

$$K_2 = \frac{4T_s}{\pi^3 L_{23}} V_2 \cos(\delta_2) V_3 \cos(\delta_3)$$

Assuming that system operation is close to point $A$ is ensured by proper pre-control (cf. Fig.12, where $\phi_{2A}$ *and* $\phi_{3A}$ is, and $\delta_{1A}$, $\delta_{2A}$, $\delta_{3A}$ could be determined based on (22)) the controller only has to slightly adjust $\phi_2$ and $\phi_3$ in a given operating region. Therefore, for deriving a control-oriented system model, (26) can be linearized at the desired operating point $A$ resulting in

$$\begin{aligned} P_2 &= P_{2A} + \Delta P_{2A} \\ &= K_{1A} \sin(\phi_{2A}) + K_{2A} \sin(\phi_{3A} - \phi_{2A}) \\ &\quad + K_{1A} \cos(\phi_{2A}) \Delta\phi_2 - K_{2A} \cos(-\phi_{3A} + \phi_{2A}) \Delta\phi_2 \\ &\quad + K_{2A} \cos(-\phi_{3A} + \phi_{2A}) \Delta\phi_3 \\ &= P_{2A} + G_{11} \Delta\phi_2 + G_{12} \Delta\phi_3 \end{aligned} \tag{27}$$

where $G_{11} = K_{1A} \cos(\phi_{2A}) - K_{2A} \cos(-\phi_{3A} + \phi_{2A})$

$$G_{12} = K_{2A} \cos(-\phi_{3A} + \phi_{2A})$$
$$P_{2A} = K_{1A} \sin(\phi_{2A}) + K_{2A} \sin(\phi_{3A} - \phi_{2A})$$

with

$$K_{1A} = -\frac{4T_s}{\pi^3 L_{12}} V_1 \cos(\delta_{1A}) V_2 \cos(\delta_{2A})$$

$$K_{2A} = \frac{4T_s}{\pi^3 L_{23}} V_2 \cos(\delta_{2A}) V_3 \cos(\delta_{3A})$$

In analogy, linearizing $P_3$ at operating point $A$ yields

$$\begin{aligned} P_3 &= P_{31} + P_{32} = -P_{13} - P_{23} \\ &= P_{3A} + \Delta P_{3A} \\ &= K_{3A} \sin(\phi_{3A}) - K_{2A} \sin(\phi_{3A} - \phi_{2A}) \\ &\quad + K_{2A} \cos(-\phi_{3A} + \phi_{2A}) \Delta\phi_2 \\ &\quad + K_{3A} \cos(\phi_{3A}) \Delta\phi_3 - K_{2A} \cos(-\phi_{3A} + \phi_{2A}) \Delta\phi_3 \\ &= P_{3A} + G_{21} \Delta\phi_2 + G_{22} \Delta\phi_3 \end{aligned} \tag{28}$$

where $G_{21} = K_{2A} \cos(-\phi_{3A} + \phi_{2A})$

$$G_{22} = K_{3A} \cos(\phi_{3A}) - K_{2A} \cos(-\phi_{3A} + \phi_{2A})$$
$$P_{3A} = K_{3A} \sin(\phi_{3A}) - K_{2A} \sin(\phi_{3A} - \phi_{2A})$$

with

$$K_{3A} = -\frac{4T_s}{\pi^3 L_{12}} V_1 \cos(\delta_{1A}) V_3 \cos(\delta_{3A}) .$$

In summary, we have for the small signal model of the system

$$\begin{bmatrix} \Delta P_2 \\ \Delta P_3 \end{bmatrix} = \begin{bmatrix} G_{11} & G_{12} \\ G_{21} & G_{22} \end{bmatrix} \begin{bmatrix} \Delta\phi_2 \\ \Delta\phi_3 \end{bmatrix} = G \begin{bmatrix} \Delta\phi_2 \\ \Delta\phi_3 \end{bmatrix} \tag{29}$$

The interaction of the control loops (29) can now be eliminated

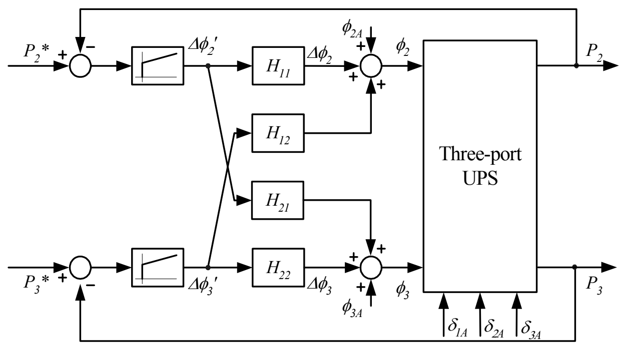


**Fig.14:** System power control employing a decoupling network. $P_2^*$ and $P_3^*$ are the power reference signals. System operation close to the optimum operating point $A$ is ensured by pre-control signals $\phi_{2A}$, $\phi_{3A}$, and $\delta_{1A}$, $\delta_{2A}$, $\delta_{3A}$.

using a decoupling network $H$ (cf. e.g., [11]). The resulting control structure is depicted in Fig.14. Based on

$$\begin{bmatrix} \Delta P_2 \\ \Delta P_3 \end{bmatrix} = GH \begin{bmatrix} \Delta\phi_2' \\ \Delta\phi_3' \end{bmatrix} \tag{30}$$

the decoupling matrix can be found as

$$\begin{aligned} H &= \begin{bmatrix} H_{11} & H_{12} \\ H_{21} & H_{22} \end{bmatrix} = G^{-1} = \begin{bmatrix} G_{11} & G_{12} \\ G_{21} & G_{22} \end{bmatrix}^{-1} \\ &= \frac{1}{G_{11}G_{22} - G_{12}G_{21}} \begin{bmatrix} G_{22} & -G_{12} \\ -G_{21} & G_{11} \end{bmatrix} \end{aligned} \tag{31}$$

## V. SIMULATION RESULTS

The above theoretical considerations have been verified by digital simulations using PSIM based on the circuit schematic shown in **Fig.15** assuming the following operating parameters and component values: $V_1$ = 500V, $V_2$ = 400V, $V_3$ = 360V, $L_1 = L_2 = L_3$ = 100µH, $f_s$ = 20kHz, $C_1 = C_2 = C_3$ = 2µF.

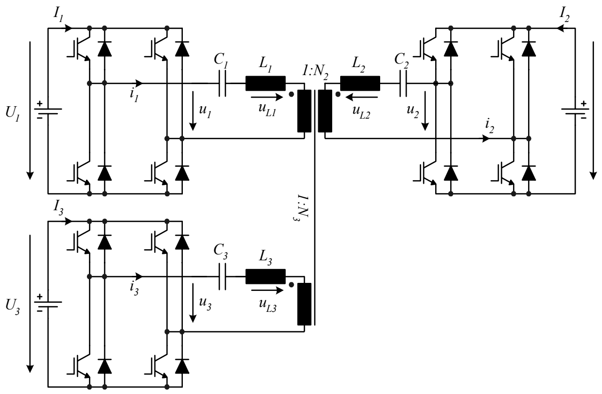


**Fig.15:** Circuit schematic employed for the circuit simulation.

The simulated system control behavior is shown in **Fig.16**. At $t$=0 the power reference signals are $P_2^*$=−3kW and $P_3^*$=−1kW (a negative power value indicates that power is absorbed by the corresponding port and/or converter cell, in the case at hand power is delivered from port 1 to ports 2 and 3). The power reference signal $P_2^*$ is stepped to −4kW at $t$=0.02s and $P_3^*$ is stepped to 0 at $t$=0.07s. The control shows excellent dynamics and only a weak cross-coupling of the control loops is remaining. A detailed description of the dynamic modeling of the system and the extension of the basic control structure to controlling $V_2$ and the battery charging current $I_2$ will be discussed in a future paper.

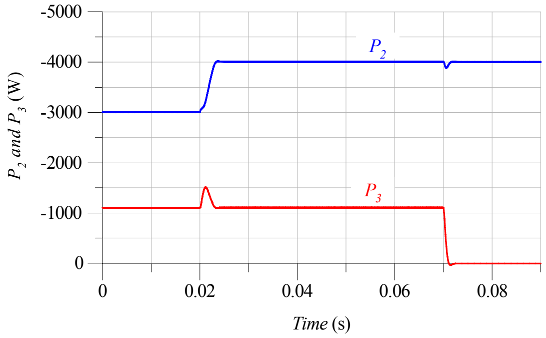


**Fig.16:** Simulation of the system control behavior for $V_1$=500V, $V_2$=400V, $V_3$=360V, $L_1$=$L_2$=$L_3$=100µH, and $f_s$=20kHz. At $t$=0 the power reference signals $P_2$* and $P_3$* are −3kW and −1kW. At $t$=0.02s $P_2$* is stepped to −4kW, and $P_3$* is stepped to 0 at $t$=0.07s.

## VI. CONCLUSIONS

A novel *Three-Port UPS* formed by linking a three-phase PWM rectifier, a three-phase PWM inverter and a battery energy storage via a single three-winding isolation transformer and corresponding full-bridge converter cells is proposed.

According to the theoretical analysis and simulation results the converter system shows the following features:

1) The bidirectional power flow between the ports can controlled by the phase-shift of the individual full-bridge cells;
2) A utilization of duty cycle control allows to operate the system with minimum power semiconductor losses
3) For employing a decoupling network, the power of the ports can be controlled independently, where operation of the system in the optimum region is ensured by proper pre-control derived from analyzing the system behavior with restriction to the fundamentals of the voltages and currents.

In a next step a DSP-controlled 5kW laboratory model of the system shown in Fig.1 will be realized for verifying the proposed control concept. Furthermore, the optimization of the system behavior will be extended to a proper selection of $V_1$ and $V_2$ for a given operating point.

## REFERENCES


[1] **N. Blacha**, "The Perspectives of UPS and Fuel Cells on the Base of a New Flexible Modular UPS Technology," in *Proc. Power Quality of PCIM 2003 conf.*, pp 21-27.

[2] **J.W. Kolar, and C. Zhao**, "Vorrichtung zur hochfrequent-potentialgetrennten bidirektionalen Kopplung von Dreiphasensystemen und Gleichspannungsquellen (in German)," *Swiss Patent Application*, filed: April 2004.

[3] **G. Chen, D. Xu, Y. Wang, and Y. Lee**, "A New Family of Soft-Switching Phase-Shift Bidirectional DC-DC Converter," in *Proc. IEEE Power Electronics Specialists Conference (PESC) 2001 conf.*, vol.2, pp 859-865.

[4] **J.C. Han, and N.E. Prasad**, "A Three-Phase AC/AC High-Frequency Link Matrix Converter for VSCF Applications," in *Proc. IEEE Power Electronics Specialists Conference (PESC) 2003 conf.*, vol.4, pp 1971-1976.

[5] **Y. Hayashi, T. Ise, and K. Tsuji**, "Power Converter System for Flexible, Reliable and Intelligent Electrical eNergey Delivery System," in *Proc. 10th European Conference on Power Electronics and Applications (EPE) 2003 conf.*, CD-ROM, ISBN: 90-75815-07-7.

[6] **A.G. Ganz**, "A simple, exact equivalent circuit for the three-winding transformer," *IRE Trans. Component parts*, vol. 9, issue 4, pp 212-213, December, 1962.

[7] **MIT Staff**, *Magnetic Circuits and Transformers*, John Wiley and Sons, Inc., New York, 1943.

[8] **N. Schibli, A. Rufer**, "Single- and Three- Phase Multilevel Converters for Traction Systems 50Hz / 16²/₃Hz," in *Proc 7th European Conference on Power Electronics and Applications (EPE) 1997 conf.*, pp 4210-4215.

[9] **W. Holger, S. Volker, and S. Andreas**, "A Soft-Switched Dual Active Bridge 3DC-to-1DC Converter employed in a High-Voltage Electronic Power Transformer," in *Proc. 10th European Conference on Power Electronics and Applications (EPE) 2003 conf.*, CD-ROM, ISBN: 90-75815-07-7.

[10] **F. Schafmeister, S. Herold, J.W. Kolar,** "Evaluation of 1200V-Si-IGBTs and 1300V-Sic-JFETs for Application in Three-Phase Very Sparse Matrix AC-AC Converter Systems," in *Proc. IEEE Applied Power Electronics Conference and Exposition (APEC) 2003 conf.*, vol.1, pp. 241-255.

[11] **W.L. Luyben**, "*Distillation Decoupling*," *Journal AIChE*, vol. 16-2, pp. 198-203, 1970